Electronic Supplementary Material (ESI) for Nanoscale.

Supplementary Information: Effect of dopamine-functionalization, charge and pH on protein corona formation around TiO_2 nanoparticles

Paulo Siani and Cristiana Di Valentin

Dipartimento di Scienza dei Materiali, Università di Milano Bicocca
Via Cozzi 55, 20125 Milano Italy

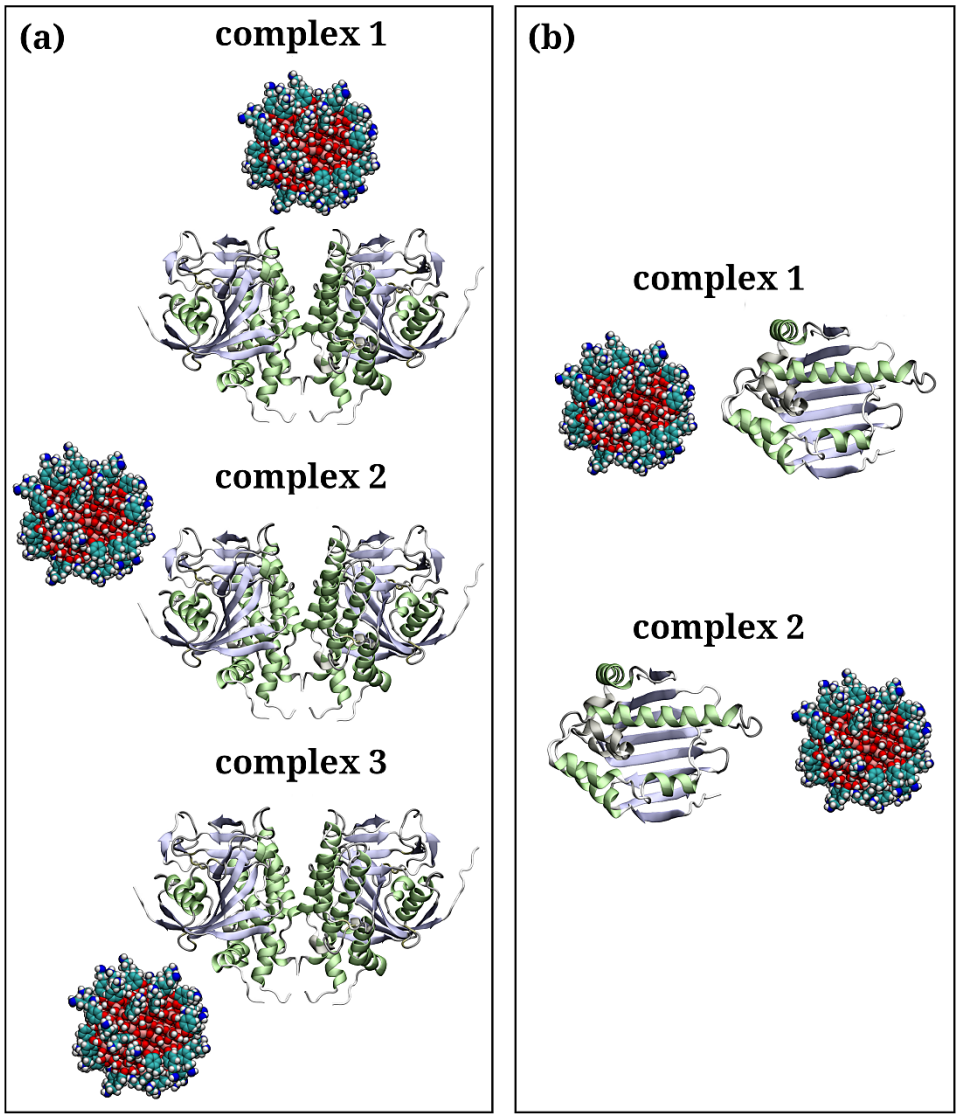

Figure S1. Starting-point structures for (a) PARP1- and (b) HSP90-NP complexes carried out using implicit solvent MD simulations.

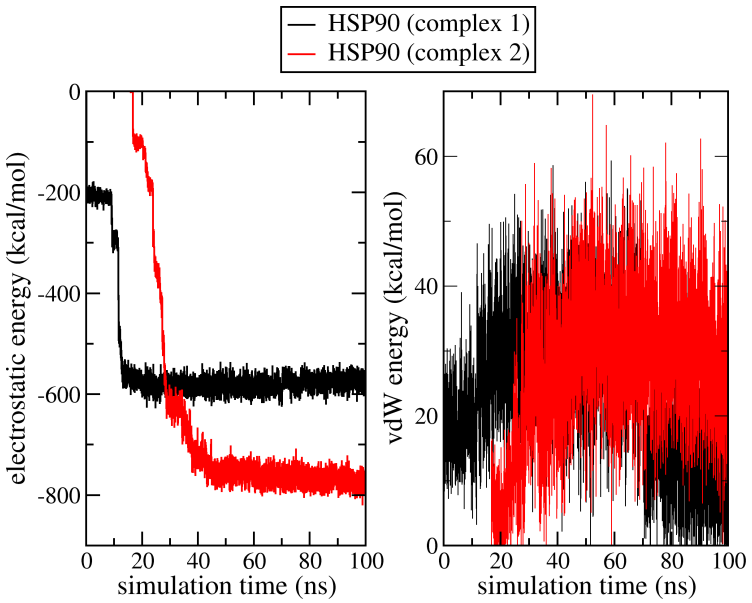

Figure S2. (left-hand side) Electrostatic and (right-hand side) vdW interaction energies between HSP90 and NP over 100 ns of implicit solvent MD simulations. The following color codes are used: (black) HSP90-NP complex 1, and (red) HSP90-NP complex 2.

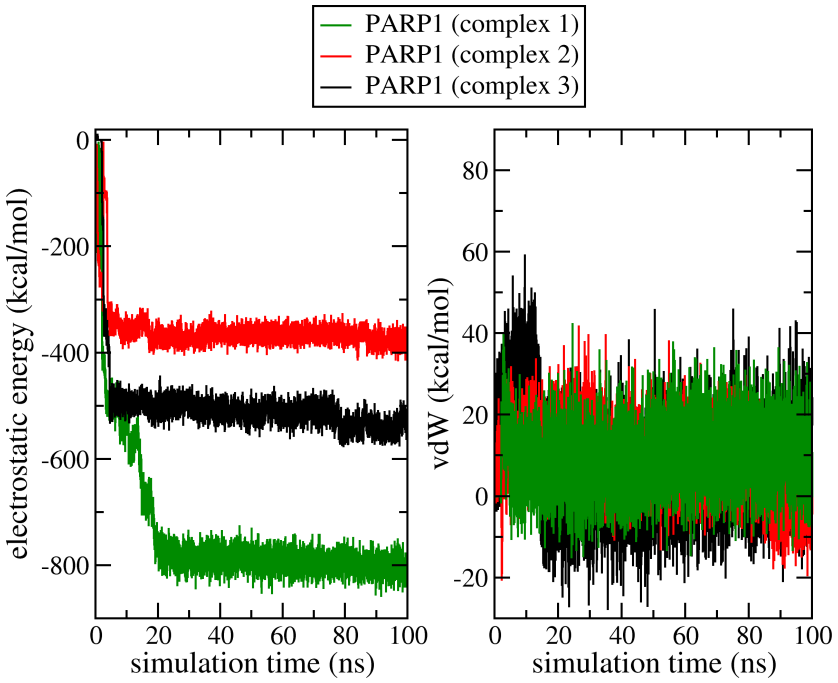

Figure S3. (left-hand side) Electrostatic and (right-hand side) vdW interaction energies between PARP1 and NP over 100 ns of implicit solvent MD simulations. The following color codes are used: (green) PARP1-NP complex 1, (red) PARP1-NP complex 2, and (black) PARP1-NP complex 3.

Table S1. Total interaction energy and its electrostatic and vdW components for the PARP1- and HSP90-NP complexes averaged over the last 50 ns of MD production. Energy unit in (kcal/mol).

PARP1-NP/(kcal/mol)	<elec>	<vdW>	Total energy
Complex 1	-497.7 (±81.8)	9.1 (±8.4)	-488.6
Complex 2	-358.5 (±45.7)	8.5 (±8.3)	-350.0
Complex 3	-633.2 (±140.0)	26.3 (±17.2)	-606.9

HSP90-NP/(kcal/mol)	<elec>	<vdW>	Total energy
Complex 1	-536.7 (±115.7)	23.8 (±11.1)	-512.9
Complex 2	-560.1 (±304.6)	22.6 (±14.8)	-537.5

Table S2. MD descriptors for the HSP90- and PARP1-NP complexes under explicit TIP3P water solvation in absence of salt averaged over the last 50 ns of MD production. Force unit in (kcal mol^{-1} $Å^{-1}$), Surface area in ($Å^2$), and Energy (kcal/mol).

Complex	<forces>	<surface area>	<elec>	<vdW>
HSP90_DA^0	52.6 (±17.0)	417.2 (±30.2)	-323.6 (±35.7)	-46.3 (±8.0)
HSP90_DA^+	91.6 (±25.7)	447.8 (±32.3)	-654.6 (±55.0)	-9.6 (±9.6)
PARP1_DA^0	36.1 (±13.1)	270.1 (±34.2)	-143.3 (±11.6)	-44.1 (±5.4)
PARP1_DA^+	51.4 (±16.8)	166.0 (±30.7)	-317.5 (±35.4)	7.9 (±6.3)
PARP1_bare	28.0 (±11.8)	472.8 (±88.0)	-148.8 (±25.7)	-83.8 (±20.9)

Table S3. MD descriptors for the HSP90- and PARP1-NP complexes under explicit TIP3P water solvation at 0.15 M of KCl concentration averaged over the last 50 ns of MD production. Force unit in (kcal mol^{-1} $Å^{-1}$), Surface area of contact in ($Å^2$), and Energy (kcal/mol).

Complex	<forces>	<surface area>	<elec>	<vdW>
HSP90_DA^0	41.5 (±15.7)	383.4 (±48.1)	-263.8 (±32.1)	-31.8 (±8.2)
HSP90_DA^+	61.1 (±17.0)	314.5 (±16.6)	-445.5 (±32.0)	-18.0 (±6.3)
PARP1_DA^0	22.1 (±8.12)	320.3 (±54.8)	-87.9 (±13.4)	-34.8 (±7.9)
PARP1_DA^+	59.8 (±16.4)	170.7 (±26.9)	-374.0 (±45.0)	1.8 (±7.3)

Table S4. Variation on MD descriptors due to the addition of 0.15 M of KCl in solution. Force unit in (kcal mol^{-1} $Å^{-1}$), Surface area of contact in ($Å^2$), and Energy (kcal/mol).

Complex	<forces>	<surface area>	<elec>	<vdW>
HSP90_DA^0	-21.1%	-8.1%	+18.5%	+31.3%
HSP90_DA^+	-33.3%	-29.8%	+31.9%	-87.5%
PARP1_DA^0	-38.8%	+18.6%	+38.7%	+21.1%
PARP1_DA^+	+16.3%	+2.8%	-17.8%	-77.2%

Table S5. Secondary structure of PARP1- and HSP90-only in the absence of NPs under TIP3P water solvation estimated over the last 50 ns of MD production phase. (a) secondary structure of PARP1 or HSP90 residues contributing to the protein corona under physiological pH conditions in Table S6, (b) secondary structure of PARP1 and HSP90 residues contributing to the protein corona under alkaline pH conditions.

Protein	β-turn	extended	isolated	α-helix	3_{10}-helix	pi-helix	coil
PARP1 (a)	49.4%	12.0%	0.0%	37.5%	0.0%	0.0%	1.1%
PARP1 (b)	12.4%	0.0%	0.1%	14.3%	0.0%	0.0%	73.2%
HSP90 (a)	34.5%	2.0%	0.1%	0.0%	0.6%	0.0%	62.8%
HSP90 (b)	7.7%	14.0%	0.0%	3.7%	0.5%	0.0%	74.1%

Table S6. Secondary structure of PARP1 and HSP90 corona motifs adsorbed onto cationic and neutral NPs under TIP3P water solvation estimated over the last 50 ns of MD production phase. (a) physiological pH conditions, (b) alkaline pH conditions.

Protein	β-turn	extended	isolated	α-helix	3_{10}-helix	pi-helix	coil
PARP1 (a)	44.4%	0.0%	0.0%	36.5%	0.0%	0.0%	19.1%
PARP1 (b)	29.6%	0.0%	0.0%	13.9%	0.0%	0.0%	56.5%
HSP90 (a)	22.0%	0.2%	0.0%	0.0%	0.0%	0.0%	77.8%
HSP90 (b)	35.3%	8.3%	0.0%	0.0%	0.0%	0.0%	56.4%

Table S7. Secondary structure of PARP1 and HSP90 corona motifs adsorbed onto cationic and neutral NPs under TIP3P water solvation at 0.15 M of KCl estimated

over the last 50 ns of MD production phase. (a) physiological pH conditions, (b) alkaline pH conditions.

Protein	β-turn	extended	isolated	α-helix	3_{10}-helix	pi-helix	coil
PARP1 (a)	8.9%	0.0%	0.0%	43.4%	0.0%	0.0%	47.7%
PARP1 (b)	25.0%	0.0%	0.0%	39.0%	0.0%	3.1%	32.9%
HSP90 (a)	16.6%	15.5%	0.9%	0.0%	0.0%	0.0%	67.0%
HSP90 (b)	34.9%	12.4%	0.1%	0.0%	0.0%	0.0%	52.6%

Table S8. Angular orientation of the NP to the protein corona residues in PARP1 and HSP90 averaged over the last 50 ns of explicit solvent MD simulations in the absence and presence of ionic strength at 0.15 M of KCl.

Complex	SALT	NO SALT
HSP90_DA^0	66.3° (±52.3)	61.3° (±10.3)
HSP90_DA^+	66.6° (±39.7)	50.1° (±3.8)
PARP1_DA^0	45.4° (±3.3)	39.7° (±33.8)
PARP1_DA^+	122.3° (±31.7)	69.3° (±1.1)
PARP1_bare	-	38.1° (±2.2)

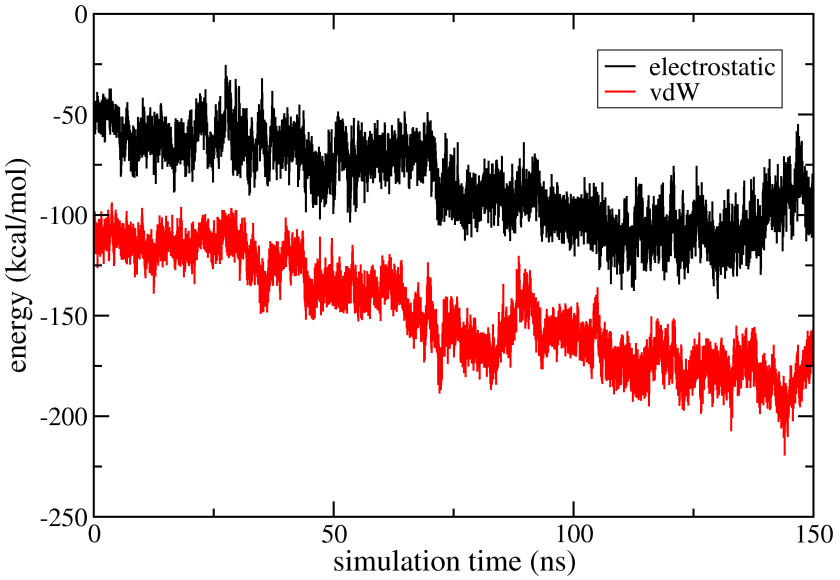

Figure S4. Electrostatic and vdW interaction energies between PARP1 and the bare NP over 150 ns of explicit solvent MD simulation.

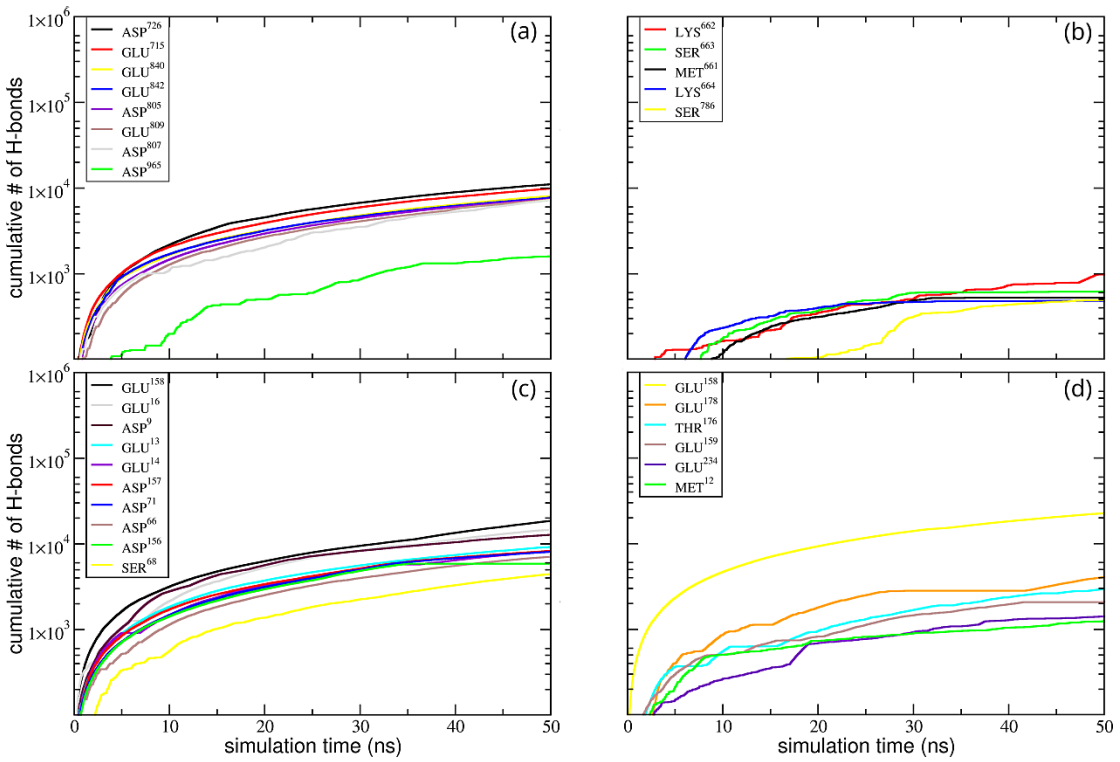

Figure S5. Cumulative number of H-bond formation between (a,b) PARP1 and (c,d) HSP90 and (a,c) cationic and (b,d) neutral NP in the absence of ionic strength. (a) PARP1-NP complex at pH 7.4, (b) PARP1-NP complex at pH 11.5, (c) HSP90-NP complex at pH 7.4, (d) HSP90-NP complex at pH 11.5.

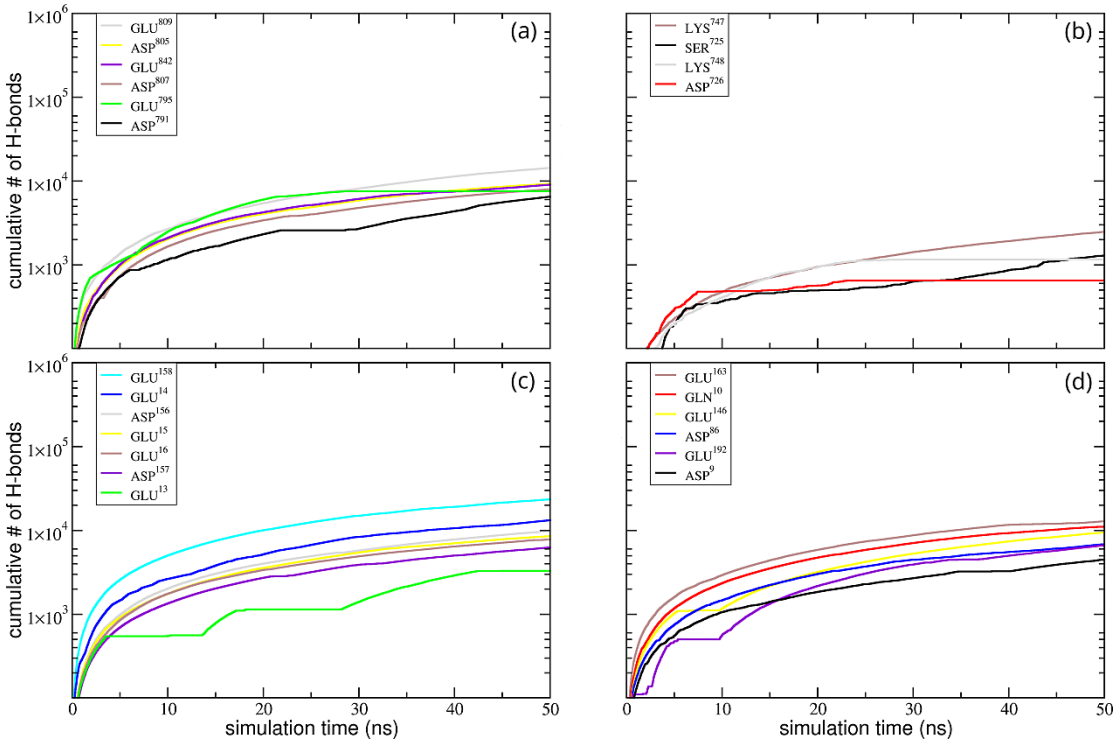

Figure S6. Cumulative number of H-bond formation between (a,b) PARP1 and (c,d) HSP90 and (a,c) cationic and (b,d) neutral NP under physiological ionic strength conditions (KCl at 0.15 M). (a) PARP1-NP complex at pH 7.4, (b) PARP1-NP complex at pH 11.5, (c) HSP90-NP complex at pH 7.4, (d) HSP90-NP complex at pH 11.5.

S1. Simulations of PARP1 interacting with non-functionalized TiO_2 NP.

To better understand how the absence of surface functionalization might affect the protein corona formation, we simulate PARP1 in the presence of a bare NP (net charge set to zero) under explicit TIP3P water solvation. The protonation state of PARP1's residues at physiological pH and the MD simulation setup follow the same protocol as reported in Section 2, manuscript. It is important to mention that no pre-treatment using implicit MD simulations has been carried out in these calculations, and the simulation time has been extended up to 150 ns. We see that the surface extent of PARP1 formed onto the bare NP is the largest one (~ 473 Å) among all protein-NP complexes reported in this work (Table S2). Compared to the functionalized NPs, we observe a substantial vdW stabilization upon PARP1 corona formation on the bare NP surface, whereas the electrostatic contribution becomes less relevant in the nonbonded interactions between PARP1 and the bare NP. Moreover, we observe an angular orientation of about 38 °, therefore, favoring the closeness of the north pole of bare NP towards the PARP1 corona residues (Table S8) compared to its equatorial region. Based on the results above, we can infer that the absence of NP functionalization by DA ligands increases the extent of PARP1 corona on the bare NP surface. Moreover, the energetic analysis reveals that the short-range vdW interactions play a significant role, whereas it is less evident in the presence of DA ligands grafted on the NP surface.

S2. Native Contacts analysis. We count as a "native contact" any pair of atoms belonging to two distinct groups of atoms (in our case, Group 1: protein atoms and Group 2: nanoparticle atoms) closer than a predefined cutoff of 3.5 Å. In other words, we are counting the number of intermolecular contacts between the protein and the nanoparticle closer than a cutoff of 3.5 Å over the last 50 ns of the MD production phase.

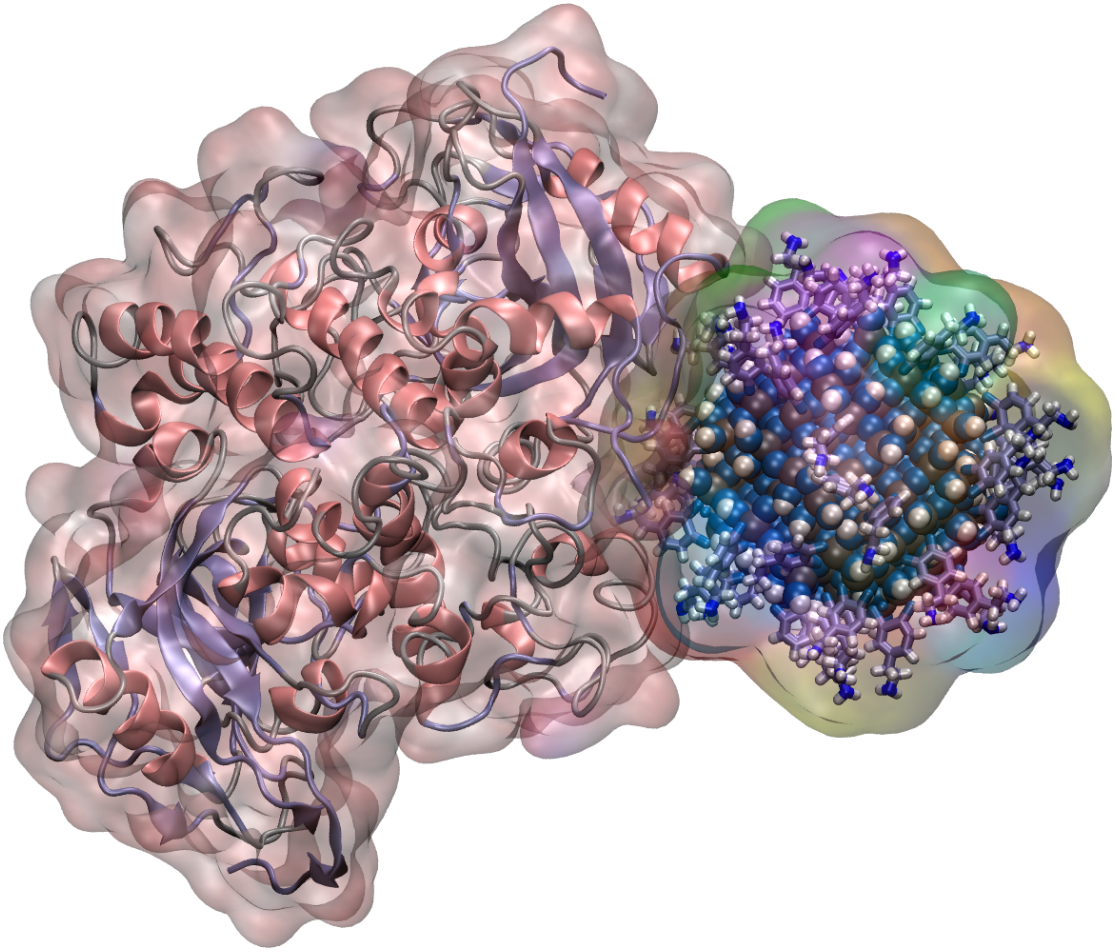

Figure S7. Final snapshot after 300 ns of explicit solvent MD simulation of the PARP1/dopamine-decorated TiO2 nanoparticle at alkaline pH conditions.